# Alkaline Earth-metal ions transfer in cell membrane through [SiO-GeO] or [SiO-SnO] nanoclusters: A biomaterials modeling investigation

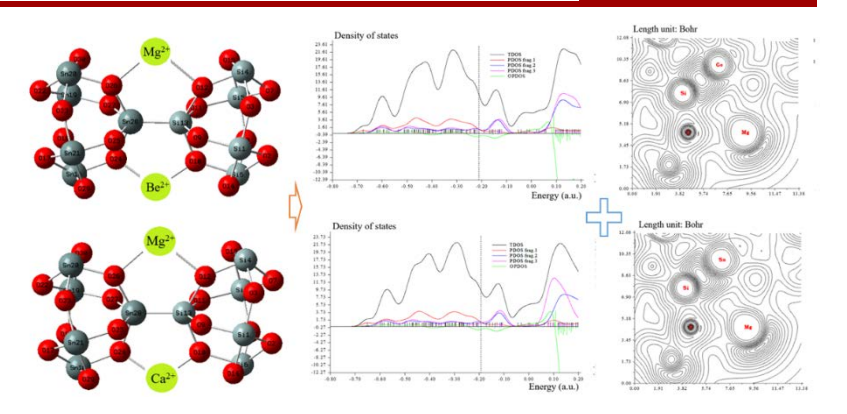
Fatemeh Mollaamin,1\* Majid Monajjemi2

Submitted on: 11-May-2025, Revised:04-Jul-2025, Accepted on:04-Jul-2025, Published on: 07-Jul-2025

Article

#### ABSTRACT

Ge,Sn/Si-based nanoparticles are used as excipients in pharmaceutical technology. Recently, silicon/germanium oxide has emerged as drug delivery systems. Therefore, in this article, it has been evaluated the promising alternative alkaline earth metals of beryllium-ion, magnesium-ion, calcium-ion delivery. This paper reports the presence of human cells of an additional ouabain-insensitive transport pathway for Mg<sup>2+</sup>–Be<sup>2+</sup> and Mg<sup>2+</sup>–Ca<sup>2+</sup> and ions cotransport. A vast



study on H-capture by Mg<sup>2+</sup>Be<sup>2+</sup> [SiO–(GeO/SnO)] or Mg<sup>2+</sup>Ca<sup>2+</sup> [SiO–(GeO/SnO)] complexes was probed using computational approaches due to density state analysis of charge density differences (CDD), total density of state (TDOS), localized orbital locator (LOL) for heteroclusters of Mg<sup>2+</sup>Be<sup>2+</sup> [SiO–GeO], Mg<sup>2+</sup>Be<sup>2+</sup> [SiO–SnO], Mg<sup>2+</sup>Ca<sup>2+</sup> [SiO–GeO] and Mg<sup>2+</sup>Ca<sup>2+</sup> [SiO–SnO]. Higher Ge/Sn to Si content can increase cell capacity through Mg<sup>+</sup>Be<sup>+</sup> [SiO–GeO], Mg<sup>2+</sup>Be<sup>2+</sup> [SiO–SnO], Mg<sup>2+</sup>Ca<sup>2+</sup> [SiO–GeO] and Mg<sup>2+</sup>Ca<sup>2+</sup> [SiO–SnO] nanoclusters for ion adsorption process and might improve the rate performances by enhancing electrical conductivity. Besides, [SiO–(GeO/SnO)] anode material may advance cycling consistency by excluding electrode decline and augments the capacity owing to higher surface capacitive impacts. The fluctuation in charge density values demonstrates that the electronic densities were mainly located in the boundary of adsorbate/adsorbent atoms during the adsorption status. Among these, beryllium-ion, magnesium-ion, calcium-ion transfer seems to show the most promise in terms of initial capacity. This ion transport can create and maintain an electrochemical gradient, which is crucial for various cellular processes, including cell volume regulation, electrical excitability, and secondary active transport. Current study wants to discover deeper into several aspects of this molecular entity, such as describing its structure and mode of operation in atomic detail, understanding its molecular and functional diversity, and examining the consequences of its malfunction due to structural alterations.

Keywords:  $Mg^{2+}$ – $Be^{2+}$  &  $Mg^{2+}$ – $Ca^{2+}$ ; ion transport, Si–Ge/Sn oxide; density of states; cell membrane

### INTRODUCTION

The lithium ions are prominently represented in the environment, however, lithium ions are not essential co-factors in biological systems. In contrast, sodium, potassium, calcium and magnesium are essential co-factors in multiple biological systems, and others such as iron, zinc, and copper play a role in some specific systems. Thus, lithium ions appear to have been isolated from being incorporated as an essential element during the evolution of increasingly complex biological systems [1–7].

The targeted delivery of therapeutics to internal organs to, for example, promote healing or apoptosis holds promise in the treatment of numerous diseases. Currently, the prevailing delivery modality relies on the circulation; however, this modality has substantial efficiency, safety and/or controllability limitations [8].

It is relevant to remark that Si-based inorganic compounds have been extensively examined for lithium-ion batteries (LIBs) [9]. Similarly, although Si-based polymer-derived ceramics (PDCs) have already been investigated as electrodes in rechargeable LIBs, [10] there are no results to discover their potential for magnesium-ion batteries (MIBs). One hopping anode material for LIBs is silicon (Si), with a theoretical capacity nearly ten times that of graphite [11]. However, the usage of Sianodes remains moderate because of magnificent volume expansion and pulverization during cell cycling, conducting

\*Corresponding Author: Prof. Fatemeh Mollaamin Email: fmollaamin@kastamonu.edu.tr



DOI:10.62110/sciencein.mms.2025.v12.1195 URN:NBN:sciencein.mms.2025.v12.1195 © Authors, The ScienceIn https://pubs.thesciencein.org/jmns



<sup>&</sup>lt;sup>1</sup> Department of Biomedical Engineering, Faculty of Engineering and Architecture, Kastamonu University, Kastamonu, Turkey.

<sup>&</sup>lt;sup>2</sup>Department of Biology, Faculty of Science, Kastamonu University, Kastamonu, Turkey.

structural deterioration and poor performance stability [9]. The extracted polymers from ceramics, especially with silicon backbone, might be a supreme candidate to modify the mentioned concerns [10]. Therefore, SiOC with Si tetrahedrally coordinated to O and C, has already been studied as electrodes in rechargeable lithium-ion batteries [12–15].

Moreover, Sn-containing SiOC/Sn nanobeads are synthesized with various C/Sn elements and examined as electrodes for Mg-ion batteries [16].

Owing to low electrical conductivity, additives such as tin (Sn) are provided to ameliorate the cycling consistency, rate performance of SiOC electrodes and reversible capacity [17,18]. It should also be underlined that, like silicon electrodes, metallic tin electrodes endure severe volume expansion and particle assossiation, conducting to poor cycling consistency [19]. Therefore, SiOC ceramics are appropriate active matrices to buffer volume alteration and density of tin during cell cycling [20–23].

Lately, the carbide hybrid nanomaterils of Si-, Ge-, Sn have been proposed as occupied H<sub>2</sub>-capture substances[24–26]. Whereas the polarizability of Si is more than C atom, it is assumed that Si–C/Si nanosurface may append to compositions more intensely in hybrid to the pure C-nanostructures [27–29 The previous investigations of energy-saving devices through H-adsorption have been tailored owing to DFT calculations with a semiconductor group of Si/Ge/Sn/Pb nano-carbides [30], Mg-Al nanoalloy [31] and Al/C/Si doping of BN nanocomposite [32]. Nanomaterials with notable structures detect undertaking demands in the field of electrocatalysis, fuel cells, and energy-saving [33].

This investigation wants to delve into the feasibility of alkaline earth metal cations delivery by [SiO–GeO] or [SiO–SnO] nanocluster through formation of  $Mg^{2+}Be^{2+}[SiO–GeO]$ ,  $Mg^{2+}Be^{2+}[SiO–SnO]$ ,  $Mg^{2+}Ca^{2+}[SiO–GeO]$  or  $Mg^{2+}Ca^{2+}[SiO–SnO]$  complexes. Therefore, it was analyzed the physicochemical properties of mentioned heteroclusters. Regarding this context, [SiO–GeO] or [SiO–SnO] nanocluster was modeled with hybride alkaline earth metal cations of  $Mg^{2+}/Be^{2+}/Ca^{2+}$  as cathode materials for comparison. Following in-depth characterization, samples were measured for their performance correlated with chemical composition varations to legislate their potency for the first time in  $Mg^{2+}-Be^{2+}$  &  $Mg^{2+}-Ca^{2+}$ -batteries.

## THEORY, MATERIALS AND COMPUTATION

The aim of this study is to transport alkali metal ions of  $Mg^{2+}$ ,  $Be^{2+}$ ,  $Ca^{2+}$  by [SiO–GeO] or [SiO–SnO] nanocluster towards formation of  $Mg^{2+}Be^{2+}$ [SiO–GeO],  $Mg^{2+}Be^{2+}$ [SiO–SnO],  $Mg^{2+}Ca^{2+}$ [SiO–GeO] or  $Mg^{2+}Ca^{2+}$ [SiO–SnO] complexes (Figure 1 a,b,c,d) which can increase the ion transfer in human cells. Figure 1(a,b,c,d) has shown alkaline earth metals-based

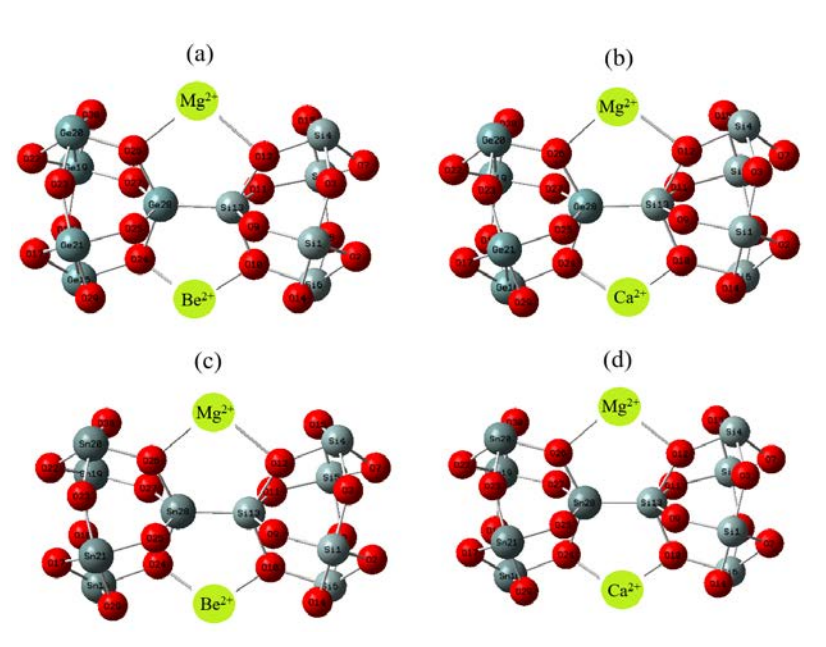


**Figure 1.** Delivery of  $Mg^{2+}$ ,  $Be^{2+}$ ,  $Ca^{2+}$  in the body cell by [SiO-(GeO/SnO)] nanoclusters and formation of (a)  $Mg^{2+}Be^{2+}$  [SiO-GeO], (b)  $Mg^{2+}Ca^{2+}$  [SiO-GeO], (c)  $Mg^{2+}Be^{2+}$  [SiO-SnO], (d)  $Mg^{2+}Ca^{2+}$  [SiO-SnO] complexes

nanoclusters of Mg<sup>2+</sup>Be<sup>2+</sup> [SiO–GeO], Mg<sup>2+</sup>Be<sup>2+</sup> [SiO–SnO], Mg<sup>2+</sup>Ca<sup>2+</sup> [SiO–GeO] and Mg<sup>2+</sup>Ca<sup>2+</sup> [SiO–SnO] which can enhance the ion delivery in bodycells, transistors or other semiconducting devices. In this investigation, the computations have been launched by Coulomb-attenuating method–(Becke, 3-parameter, Lee-Yang-Parr) [CAM–B3LYP–D3] level of theory.

The analysis of Bader charge parameter [34] has been illustrated for  $H_2$ -captured hybrid clusters of  $Mg^{2+}Be^{2+}[SiO-GeO]$ ,  $Mg^{2+}Be^{2+}[SiO-SnO]$ ,  $Mg^{2+}Ca^{2+}[SiO-SnO]$ . and  $Mg^{2+}Ca^{2+}[SiO-SnO]$ . (Figure 1a,b,c,d) due to Gaussian 16 revision C.01 computational software [35] and Gauss View 6.1 graphical program [36]. The applied basis sets for theoretical calculations of  $H_2$ -capture by  $Mg^{2+}Be^{2+}$  [SiO-GeO],  $Mg^{2+}Be^{2+}$  [SiO-SnO],  $Mg^{2+}Ca^{2+}$  [SiO-GeO] and  $Mg^{2+}Ca^{2+}$  [SiO-SnO] has been supported by LANL2DZ and 6–311+G (d,p).

One of the most significant advantages of applying (Ge/Sn)-containing SiO nanocluster as anodes/cathodes in magnesium batteries is they provide several potential Mg ion storage ways in a stable [SiO–(GeO/SnO)] anode material, increased electrical conductivity from Ge/Sn and surface area from the nanocluster morphology. In this investigation, homogenously distributed germanium or tin elements can be immobilized in the SiO matrix, which prevents their tendency to form agglomeration under cell cycling. The Mg/Be/Ca insertion might also result in the cleavage of some Si–O, Ge–O or Sn–O bonds in the [SiO–(GeO/SnO)] anode material and the expansion, providing favorable sites for the subsequent ion insertion in the network.

At the same time, the Mg, Be, Ca atoms could react rapidly with a metalloid germanium or metal tin, and possibly hybrid nanocluster of [SiO–(GeO/SnO)] to form different Mg-based alloys of  $Mg^{2+}Be^{2+}$  [SiO–GeO](Figure1a),  $Mg^{2+}Ca^{2+}$  [SiO–GeO] (Figure1b),  $Mg^{2+}Be^{2+}$  [SiO–SnO](Figure1c) and  $Mg^{2+}Ca^{2+}$  [SiO–SnO](Figure1d).

#### RESULTS AND DISCUSSION

#### 3.1. Charge density differences analysis

In Figure 2(a,b,c,d), charge density differences (CDD) [37] have been shown for  $Mg^{2+}Be^{2+}$  [SiO–GeO],  $Mg^{2+}Ca^{2+}$  [SiO–GeO],  $Mg^{2+}Be^{2+}$  [SiO–SnO],  $Mg^{2+}Ca^{2+}$  [SiO–SnO] nanoclusters with the vibration in the district about -12 to +6/+10 Bohr. Moreover, the elements of O2, O3, O7–O12, O14, O15, O17, O(18), O22–O27, O29, O30 from Mg-based alloys of  $Mg^{2+}Be^{2+}$  [SiO–GeO],  $Mg^{2+}Ca^{2+}$  [SiO–GeO],  $Mg^{2+}Be^{2+}$  [SiO–SnO],  $Mg^{2+}Ca^{2+}$  [SiO–SnO] have displayed the vibration about -12 to +6/+10 Bohr (Figure 2a,b,c,d).

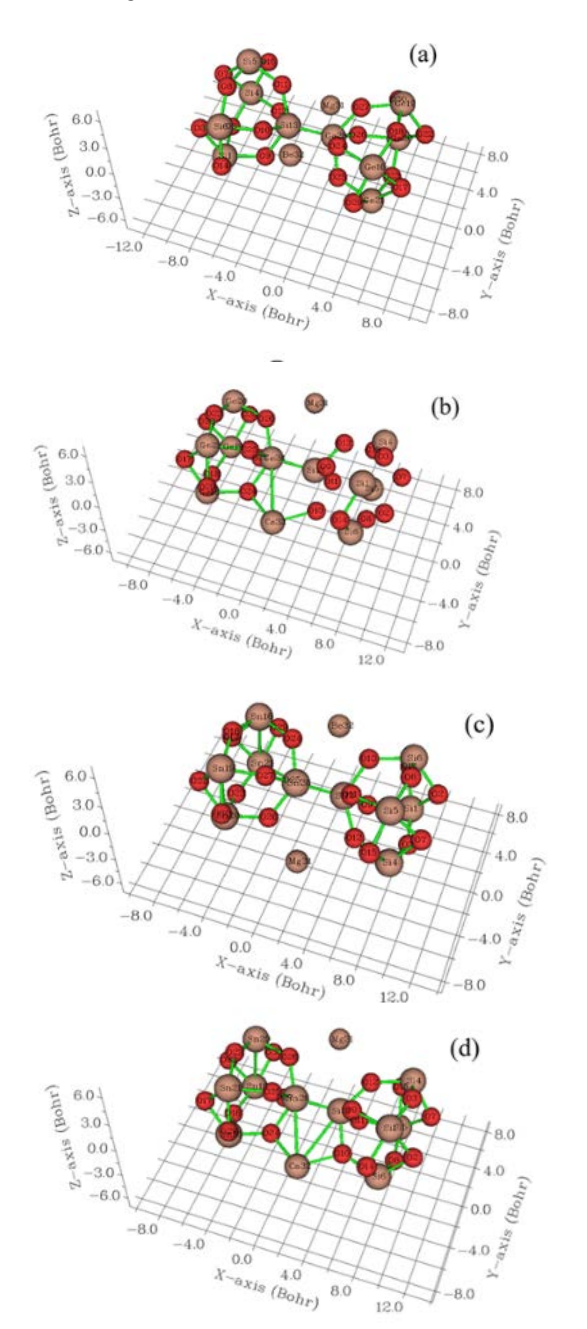


**Figure 2.** CDD graphs for (a)  $Mg^{2+}Be^{2+}$  [SiO–GeO], (b)  $Mg^{2+}Ca^{2+}$  [SiO–GeO], (c)  $Mg^{2+}Be^{2+}$  [SiO–SnO], (d)  $Mg^{2+}Ca^{2+}$  [SiO–SnO], nanoclusters.

The charge distribution has been illustrated by  $Mg^{2+}Be^{2+}[SiO-GeO]$ ,  $Mg^{2+}Ca^{2+}[SiO-GeO]$ ,  $Mg^{2+}Be^{2+}$  [SiO-SnO],  $Mg^{2+}Ca^{2+}[SiO-SnO]$  nanoclusters (Tables 1 & 2). Functionalizing of Mg, Be, Ca atoms can augment the negative atomic charge of O2, O3, O7–O12, O14, O15, O17, O(18), O22–O27, O29, O30 in  $Mg^{2+}Be^{2+}$  [SiO-GeO],  $Mg^{2+}Ca^{2+}$  [SiO-GeO],  $Mg^{2+}Be^{2+}$  [SiO-SnO] nanoclusters.

**Table 1.** The atomic charge (Q/coulomb) for  $Mg^{2+}Be^{2+}$  [SiO–GeO],  $Mg^{2+}Be^{2+}$  [SiO–GeO].H<sub>2</sub>,  $Mg^{2+}Ca^{2+}$  [SiO–GeO],  $Mg^{2+}Ca^{2+}$  [SiO–GeO].H<sub>2</sub> nanoclusters.

Mg <sup>2+</sup> Be <sup>2</sup>	<sup>+</sup> [SiO–GeO]	Mg <sup>2+</sup> Ca <sup>2+</sup>	[SiO-GeO]
Atom	Q	Atom	Q
Si1	1.4393	Si1	1.4372
O2	-0.6703	O2	-0.6788
O3	-0.8343	О3	-0.8340
Si4	1.3740	Si4	1.366
Si5	1.4332	Si5	1.4286
Si6	1.4172	Si6	1.3943
O7	-0.6767	O7	-0.6763
O8	-0.8532	O8	-0.8475
O9	-0.8153	O9	-0.8197
O10	-0.9649	O10	-1.2365
011	-0.8329	O11	-0.8281
O12	-1.0175	O12	-1.0194
Si13	1.5445	Si13	1.5089
O14	-0.7512	O14	-0.7804
O15	-0.7733	O15	-0.7745
Ge16	1.3562	Ge16	1.3435
O17	-0.6284	O17	-0.6324
O18	-0.7884	O18	-0.7822
Ge19	1.3576	Ge19	1.3549
Ge20	1.3304	Ge20	1.3243
Ge21	1.3682	Ge21	1.3704
O22	-0.6836	O22	-0.6884
O23	-0.7965	O23	-0.7970
O24	-0.9093	O24	-1.1820
O25	-0.8050	O25	-0.8135
O26	-0.9793	O26	-0.9811
O27	-0.8325	O27	-0.8143
Ge28	1.2053	Ge28	1.1979
O29	-0.7461	O29	-0.7978
O30	-0.7284	O30	-0.7262
Mg31	1.2824	Mg31	1.2514
Be32	0.9790	Ca32	1.7324

**Table 2.** The atomic charge (Q/coulomb) for  $Mg^{2+}Be^{2+}$  [SiO–SnO],  $Mg^{2+}Be^{2+}$  [SiO–SnO].H<sub>2</sub>,  $Mg^{2+}Ca^{2+}$  [SiO–SnO],  $Mg^{2+}Ca^{2+}$  [SiO–SnO].H<sub>2</sub> nanoclusters.

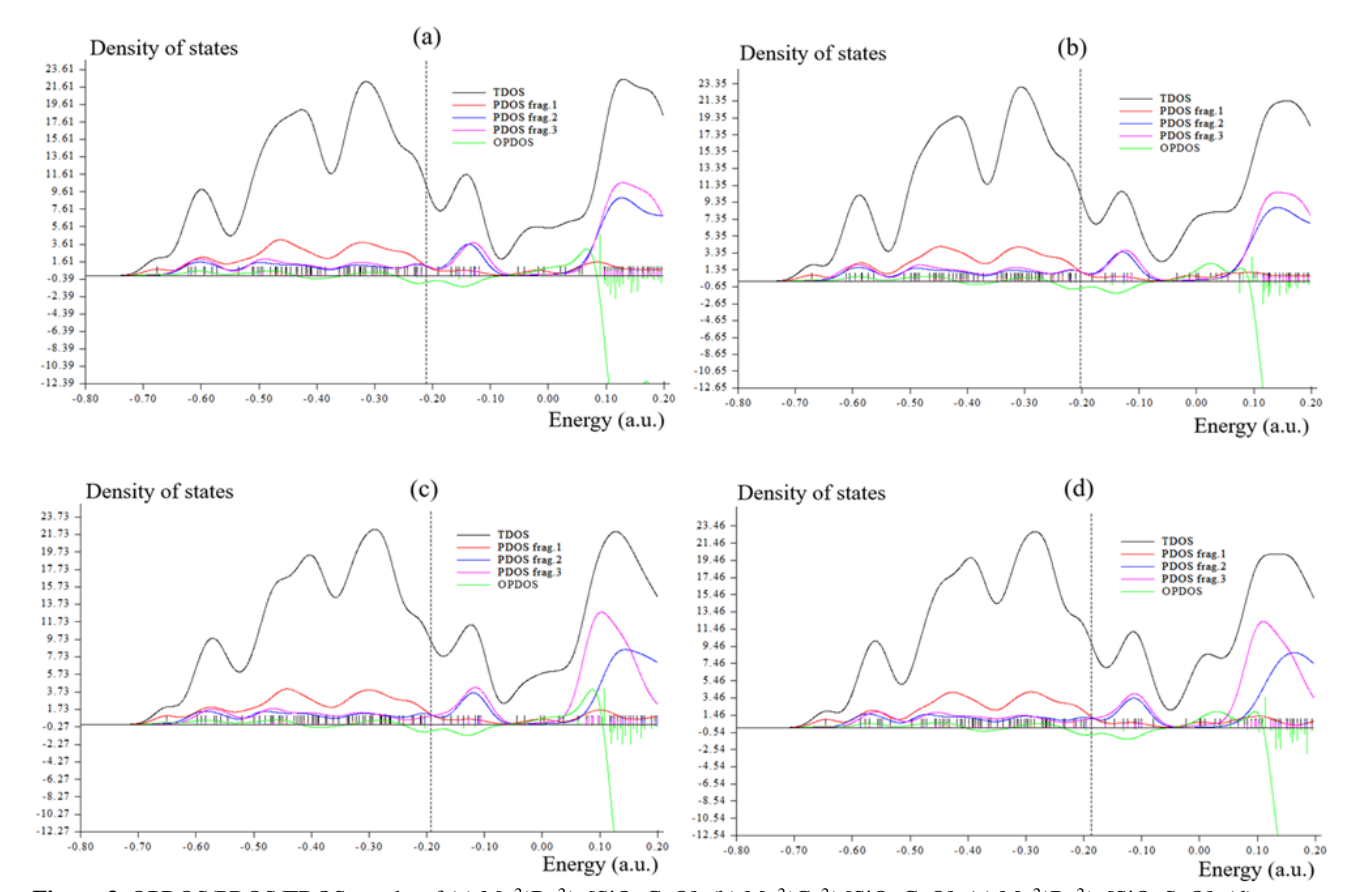
Mg <sup>2+</sup> Be <sup>2</sup>	+ [SiO-SnO]	Mg <sup>2+</sup> Ca <sup>2+</sup> [SiO–SnO]	
Atom	Q	Atom	Q
Si1	1.4285	Si1	1.4300
O2	-0.6719	O2	-0.6895
О3	-0.8351	O3	-0.8320
Si4	1.3636	Si4	1.3597
Si5	1.4168	Si5	1.4167
Si6	1.4029	Si6	1.3827
O7	-0.6886	O7	-0.6830
O8	-0.8536	O8	-0.8450
O9	-0.8227	O9	-0.8304
O10	-0.9564	O10	-1.2393
011	-0.8390	011	-0.8324
O12	-1.0083	O12	-1.0091
Si13	1.3627	Si13	1.3426
O14	-0.7749	O14	-0.8001
O15	-0.7646	O15	-0.7757
Sn16	1.6457	Sn16	1.6092
O17	-0.8062	O17	-0.7944

O18	-0.8870	O18	-0.8719
Sn19	1.6753	Sn19	1.6533
Sn20	1.6269	Sn20	1.5903
Sn21	1.6774	Sn21	1.6238
O22	-0.8309	O22	-0.8107
O23	-0.8919	O23	-0.8810
O24	-0.9885	O24	-1.2527
O25	-0.9185	O25	-0.9201
O26	-1.0596	O26	-1.0678
O27	-0.9570	O27	-0.9403
Sn28	1.6716	Sn28	1.6348
O29	-0.8873	O29	-0.9249
O30	-0.8926	O30	-0.8887
Mg31	1.1567	Mg31	1.1344
Be32	0.9065	Ca32	1.7117

# 3.2. Total Density of State

In isolated system (such as molecule), the energy levels are discrete, the concept of "density of state (DOS)" is supposed to be completely valueless in this situation. Therefore, the "original total DOS (TDOS)" of isolated system can be written as [38]:

$$TDOS(E) = \sum_{i} \delta(E - \epsilon_{i})$$
 (1)



 $\label{eq:figure 3. OPDOS/PDOS/TDOS graphs of (a) Mg$^2$+Be$^2$+ [SiO-GeO], (b) Mg$^2$+Ca$^2$+ [SiO-GeO], (c) Mg$^2$+Be$^2$+ [SiO-SnO], (d) Mg$^2$+Ca$^2$+ [SiO-SnO], nanoclusters. }$ 

The normalized Gaussian function is defined as:

$$G(x) = \frac{1}{c\sqrt{2\pi}}e^{-\frac{x^2}{2c^2}} \text{ where } c = \frac{\text{FWHM}}{2\sqrt{2\ln x}}$$
 (2)

"FWHM (full width at half maximum)" is an adjustable parameter in "Multiwfn" [39,40]. Furthermore, the curve map of "broadened partial DOS (PDOS)" and "overlap DOS (OPDOS)" are valuable for visualizing orbital composition analysis, "PDOS function of fragment *A*" is defined as:

$$PDOS_A(E) = \sum_i \Xi_{i,A} F(E - \epsilon_i)$$
 (3)

where " $\Xi_{i,A}$  is the composition of fragment A in orbital i". The "OPDOS between fragment A and B "is defined as:

$$OPDOS_{A,B}(E) = \sum_{i} X_{A,B}^{i} F(E - \epsilon_{i})$$
(4)

where " $X_{A,B}^i$  is the composition of total cross term between fragment A and B in orbital i ".

In the "TDOS map", each discrete vertical line corresponds to a "molecular orbital (MO)", the dashed line highlights the position of "HOMO". The curve is the "TDOS" simulated based on the distribution of "MO" energy levels.

Mg<sup>2+</sup>Be<sup>2+</sup> [SiO–GeO], Mg<sup>2+</sup>Ca<sup>2+</sup> [SiO–GeO], Mg<sup>2+</sup>Be<sup>2+</sup> [SiO–

SnO],  $Mg^{2+}Ca^{2+}$  [SiO-SnO] (Figure 3 a,b,c,d) have shown the steepest maximums TDOS surrounding -0.30, -0.40 and -0.60 a.u. owing to covalent bond between  $Mg^{2+}/Be^{2+}$  and  $Mg^{2+}/Ca^{2+}$  with [SiO-(GeO/SnO)] nanocluster with maximum density of state of  $\approx 22$ .

Fragment 1 has been defined for O9 to O12, Si13, O24 to O27 and Ge28,  $Mg^{2+}31/X32$ (Y=Be2+, Ca2+) in Figure3 (a-d). Fragment 2 has indicated the fluctuation of Si1. Si4 to Si6 beside the similar involved atoms of Fragment 1 in Figure 3. Finally, it was considered fluctuation Ge16/Sn16, Ge19/Sn19 to Ge21/Sn21, O17, O18, O22, O23, O29, O30 in Figure3 (a-d) through Fragment 3.

# 3.3. Localized orbital locator analysis

Localized orbital locator (LOL) has a similar expression compared to "electron localization function (ELF)" [41–43].

$$LOL(\mathbf{r}) = \frac{\tau(\mathbf{r})}{1 + \tau(\mathbf{r})}; \tau(\mathbf{r}) = \frac{D_0(\mathbf{r})}{\frac{1}{2} \sum_i \eta_i |\nabla \varphi_i(\mathbf{r})|^2}$$
 (5)

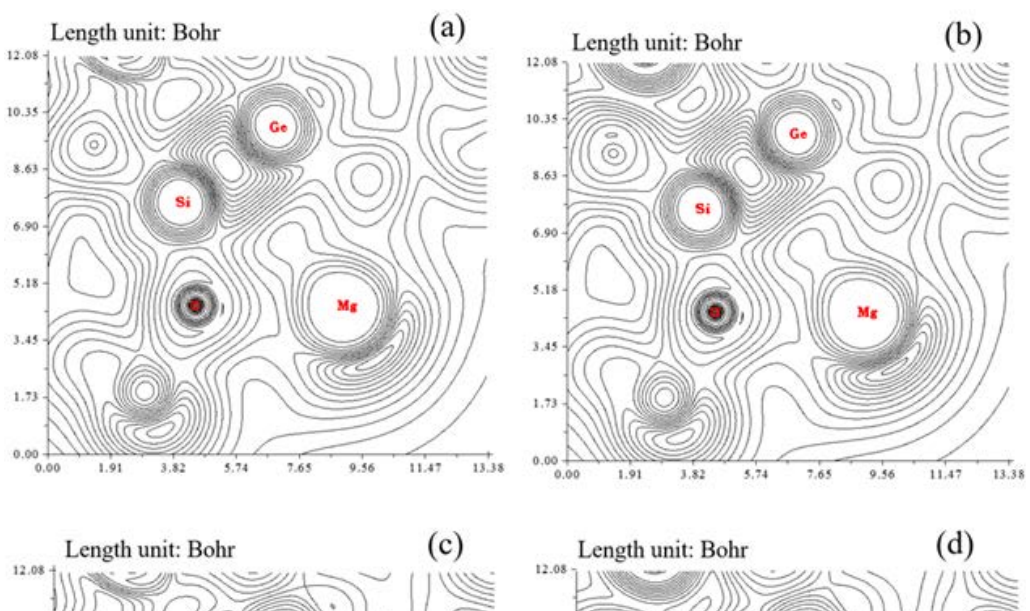
$$D_0(\mathbf{r}) = \frac{3}{10} (6\pi^2)^{2/3} \left[ \rho_{\alpha} (\mathbf{r})^{5/3} + \rho_{\beta} (\mathbf{r})^{5/3} \right]$$
 (6)

"Multiwfn" [39, 40] also supports the approximate version of "LOL" defined by "Tsirelson and Stash" [44], namely the actual kinetic energy term in "LOL" is replaced by "second-order gradient expansion like ELF" which may demonstrate a broad span of bonding samples. This "Tsirelson's version of LOL" can be activated by setting "ELFLOL\_type to 1. For special reason", if "ELFLOL\_type in settings.ini is changed from 0 to 2", another formalism will be used:

$$LOL(\mathbf{r}) = \frac{1}{1 + \left[\frac{1}{\tau(\mathbf{r})}\right]^2}$$
 (7)

If the parameter "ELFLOL\_cut in settings.ini is set to x", then "LOL will be zero where LOL is less than x".

Delivery of alkaline earth metal cations by Mg<sup>2+</sup>Be<sup>2+</sup> [SiO–GeO], Mg<sup>2+</sup>Ca<sup>2+</sup> [SiO–GeO], Mg<sup>2+</sup>Be<sup>2+</sup> [SiO–SnO], Mg<sup>2+</sup>Ca<sup>2+</sup> [SiO–SnO] nanoclusters (Figure 4a,b,c,d) might be described by LOL graphs using Multiwfn [39,40] due to achieving their



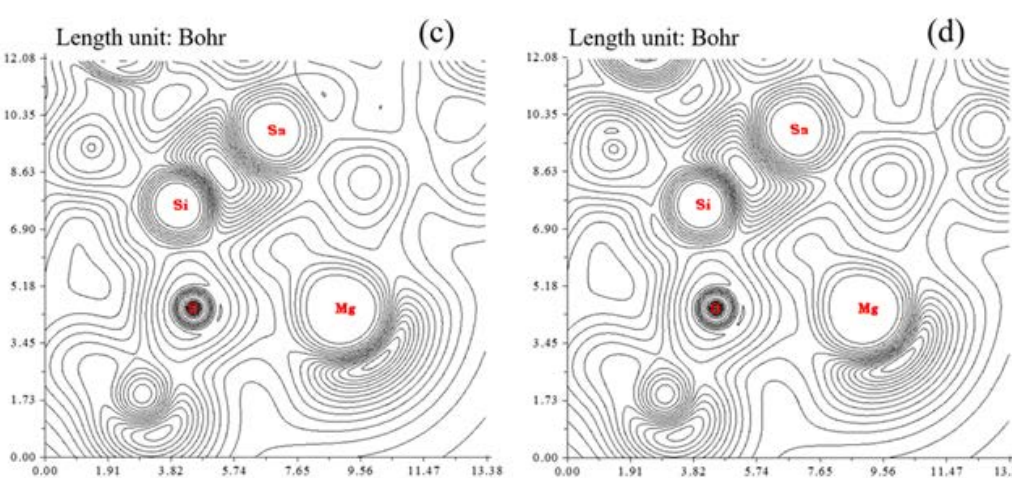


**Figure 4.** The shaded map of LOL graphs for (a)  $Mg^{2+}Be^{2+}$  [SiO–GeO], (b)  $Mg^{2+}Ca^{2+}$  [SiO–GeO], (c)  $Mg^{2+}Be^{2+}$  [SiO–SnO], (d)  $Mg^{2+}Ca^{2+}$  [SiO–SnO] nanoclusters.

delocalization/localization characterizations [41] of electrons and chemical bonds (Figure 4a,b,c,d).

 $Mg^{2+}Be^{2+}$  [SiO–GeO] (Figure 4a),  $Mg^{2+}Ca^{2+}$  [SiO–GeO] (Figure 4b),  $Mg^{2+}Be^{2+}$  [SiO–SnO] (Figure 4c),  $Mg^{2+}Ca^{2+}$  [SiO–SnO] (Figure 4d) have demonstarted the electron delocalization through an isosurface map with labeling atoms of O10, O12, Si13, O24, O26, Ge28 or Sn28,  $X(31)(X=Mg^{2+})$ , Y(32) ( $Y=Be^{2+}$  or  $Ca^{2+}$ ).

Besides, intermolecular orbital overlap integral is important in illustration of intermolecular charge transfer which can compute HOMO-HOMO and LUMO-LUMO overlap integrals between the alkaline earth metal cations of  $Mg^{2+},\ Be^{2+}$  or  $Ca^{2+}$  and heterocluster of [SiO–GeO] or [SiO–SnO] towards formation of  $Mg^{2+}Be^{2+}$  [SiO–GeO],  $Mg^{2+}Ca^{2+}$  [SiO–GeO],  $Mg^{2+}Be^{2+}$  [SiO–SnO], and  $Mg^{2+}Ca^{2+}$  [SiO–SnO] complexes. The layered germanium/tin-silicon oxide improved by alkaline earth metals of magnesium, beryllium and calcium have indicated the structural stability of  $Mg^{2+}$ -,  $Be^{2+}$ -,  $Ca^{2+}$ -ion batteries through the reported stability energy in Table 3. A small portion of  $Mg^{2+}$ ,  $Be^{2+}$  or  $Ca^{2+}$  entered the Si–Ge or Si–Sn layer to replace the alkaline earth metals sites might improve the structural stability of the electrode material at high multiplicity, thereby improving the capacity retention rate.

# **CONCLUSIONS**

Delivery of alkaline earth metal cations of  $Mg^{2+}$ ,  $Be^{2+}$  or  $Ca^{2+}$  in the body cells by heterocluster of [SiO–GeO] or [SiO–SnO] towards formation of  $Mg^{2+}Be^{2+}$  [SiO–GeO],  $Mg^{2+}Ca^{2+}$  [SiO–GeO],  $Mg^{2+}Be^{2+}$  [SiO–SnO],  $Mg^{2+}Ca^{2+}$  [SiO–SnO] complexes was studied by computational method. The changes of charge density defined a notable charge transfer in  $Mg^{2+}Be^{2+}$  [SiO–GeO],  $Mg^{2+}Ca^{2+}$  [SiO–GeO],  $Mg^{2+}Ca^{2+}$  [SiO–SnO],  $Mg^{2+}Ca^{2+}$  [SiO–SnO].

It is well established that enhancing of Mg, Be or Ca to cell batteries might augment the energy-saving in cell batteries. The results of this research article represent that the architectural design of XY(GeSiO) ( $X = Mg^{2+}/Y = Be^{2+}, Ca^{2+}$ ) can augment the capacity of body cell.

# ACKNOWLEDGEMENTS

Authors are grateful to Kastamonu University for necessary facilities for this research.

**Author Contributions:** Conceptualization, F.M.; methodology, F.M. and M.M.; software, F.M. and M.M.; validation, F.M.; formal analysis, F.M. and M.M.; investigation, F.M. and M.M.; resources, M.M.; data curation, F.M. and M.M.; writing—original draft preparation, F.M.; writing—review and editing, M.M.; visualization, F.M. and M.M.; supervision, F.M.; project administration, F.M. All authors have read and agreed to the published version of the manuscript

**Funding:** This research received no external funding.

**Conflict of interest statement**: Authors declare that there is conflict of interest for this work as no external funding was received for this work.

#### REFERENCES AND NOTES

- A. Naeem, M. Aslam, Saifullah, K.H. Mühling. Lithium: Perspectives of nutritional beneficence, dietary intake, biogeochemistry, and biofortification of vegetables and mushrooms. Sci. Total Environ. 2021, 798, 149249.
- G.N. Schrauzer. Lithium: Occurrence, Dietary Intakes, Nutritional Essentiality. J. Am. Coll. Nutr. 2002, 21 (1), 14–21.
- D.A. Hart. Lithium Ions as Modulators of Complex Biological Processes:
   The Conundrum of Multiple Targets, Responsiveness and Non-Responsiveness, and the Potential to Prevent or Correct Dysregulation of Systems during Aging and in Disease. *Biomolecules* 2024, 14 (8), 905.
- P. Dobosy, Á. Illés, A. Endrédi, G. Záray. Lithium concentration in tap water, bottled mineral water, and Danube River water in Hungary. Sci. Rep. 2023, 13 (1), 12543.
- V.J. De-Paula, O. V. Forlenza. Lithium modulates multiple tau kinases with distinct effects in cortical and hippocampal neurons according to concentration ranges. *Naunyn. Schmiedebergs. Arch. Pharmacol.* 2022, 395 (1), 105–113.
- J.R. Osete, I.A. Akkouh, O. Ievglevskyi, et al. Transcriptional and functional effects of lithium in bipolar disorder iPSC-derived cortical spheroids. *Mol. Psychiatry* 2023, 28 (7), 3033–3043.
- D. Salem, R.J. Fecek. Role of microtubule actin crosslinking factor 1 (MACF1) in bipolar disorder pathophysiology and potential in lithium therapeutic mechanism. *Transl. Psychiatry* 2023, 13 (1), 221.
- D. Yin, P. Wang, Y. Hao, et al. A battery-free nanofluidic intracellular delivery patch for internal organs. *Nature* 2025.
- X. Zhao, V.P. Lehto. Challenges and prospects of nanosized silicon anodes in lithium-ion batteries. *Nanotechnology* 2021, 32 (4), 42002.
- Q. Wen, F. Qu, Z. Yu, et al. Si-based polymer-derived ceramics for energy conversion and storage. *Journal of Advanced Ceramics*. 2022, pp 197–246.
- M. Ge, C. Cao, G.M. Biesold, et al. Recent Advances in Silicon-Based Electrodes: From Fundamental Research toward Practical Applications. *Advanced Materials*. 2021, p 2004577.
- G. Shao, D.A.H. Hanaor, J. Wang, et al. Polymer-Derived SiOC Integrated with a Graphene Aerogel As a Highly Stable Li-Ion Battery Anode. ACS Appl. Mater. Interfaces 2020, 12 (41), 46045–46056.
- G. Mera, A. Navrotsky, S. Sen, H.J. Kleebe, R. Riedel. Polymer-derived SiCN and SiOC ceramics-structure and energetics at the nanoscale. *J. Mater. Chem. A* 2013, 1 (12), 3826–3836.
- M. Wilamowska-Zawlocka, P. Puczkarski, Z. Grabowska, et al. Silicon oxycarbide ceramics as anodes for lithium ion batteries: Influence of carbon content on lithium storage capacity. RSC Advances. 2016, pp 104597–104607
- V.S. Pradeep, D.G. Ayana, M. Graczyk-Zajac, G.D. Soraru, R. Riedel. High Rate Capability of SiOC Ceramic Aerogels with Tailored Porosity as Anode Materials for Li-ion Batteries. *Electrochim. Acta* 2015, 157, 41–45
- W. Guo, O. Icin, C. Vakifahmetoglu, et al. Magnesium-Ion Battery Anode from Polymer-Derived SiOC Nanobeads. *Adv. Funct. Mater.* 2023, 33 (48), 2304933.
- C. Shi, H. Huang, Y. Xia, et al. Importing Tin Nanoparticles into Biomass-Derived Silicon Oxycarbides with High-Rate Cycling Capability Based on Supercritical Fluid Technology. *Chemistry - A European Journal*. 2019, pp 7719–7725.
- K. Kravchyk, L. Protesescu, M.I. Bodnarchuk, et al. Monodisperse and inorganically capped Sn and Sn/SnO2 nanocrystals for high-performance Li-ion battery anodes. J. Am. Chem. Soc. 2013, 135 (11), 4199–4202.
- J. Gonzalez, K. Sun, M. Huang, et al. X-ray microtomography characterization of Sn particle evolution during lithiation/delithiation in lithium ion batteries. J. Power Sources 2015, 285, 205–209.
- J. Wang, D. Kober, G. Shao, et al. Stable anodes for lithium-ion batteries based on tin-containing silicon oxycarbonitride ceramic nanocomposites. *Mater. Today Energy* 2022, 26, 100989.
- R.J.C. Dubey, P.V.W. Sasikumar, F. Krumeich, et al. Silicon Oxycarbide—Tin Nanocomposite as a High-Power-Density Anode for Li-Ion Batteries. *Advanced Science*, 2019, p 1901220.

- J. Kaspar, C. Terzioglu, E. Ionescu, et al. Stable SiOC/Sn nanocomposite anodes for lithium-ion batteries with outstanding cycling stability. *Advanced Functional Materials*. 2014, pp 4097–4104.
- D.H. Youn, A. Heller, C.B. Mullins. Simple Synthesis of Nanostructured Sn/Nitrogen-Doped Carbon Composite Using Nitrilotriacetic Acid as Lithium Ion Battery Anode. Chem. Mater. 2016, 28 (5), 1343–1347.
- W. Nazeer, A. Farooq, M. Younas, M. Munir, S.M. Kang. On molecular descriptors of carbon nanocones. *Biomolecules* 2018, 8 (3), 92.
- J. Zhao, Z. Li, M.T. Cole, et al. Nanocone-shaped carbon nanotubes field-emitter array fabricated by laser ablation. *Nanomaterials* 2021, 11 (12), 3244.
- Y. Rong, Y. Cao, N. Guo, et al. A simple method to synthesize V2O5 nanostructures with controllable morphology for high performance Liion batteries. *Electrochim. Acta* 2016, 222, 1691–1699.
- N. Yodsin, H. Sakagami, T. Udagawa, et al. Metal-doped carbon nanocones as highly efficient catalysts for hydrogen storage: Nuclear quantum effect on hydrogen spillover mechanism. *Mol. Catal.* 2021, 504, 111486
- H.O. Taha, A.M. El Mahdy, F.E.S. El Shemy, M.M. Hassan. Hydrogen storage in SiC, GeC, and SnC nanocones functionalized with nickel, Density Functional Theory—Study. *Int. J. Quantum Chem.* 2023, 123 (3), 123.
- T. Wei, Y. Zhou, C. Sun, et al. An intermittent lithium deposition model based on CuMn-bimetallic MOF derivatives for composite lithium anode with ultrahigh areal capacity and current densities. *Nano Res.* 2024, 17 (4), 2763–2769.
- F. Mollaamin, M. Monajjemi. Nanomaterials for Sustainable Energy in Hydrogen-Fuel Cell: Functionalization and Characterization of Carbon Nano-Semiconductors with Silicon, Germanium, Tin or Lead through Density Functional Theory Study. Russ. J. Phys. Chem. B 2024, 18 (2), 607–623.
- F. Mollaamin, S. Shahriari, M. Monajjemi. Influence of Transition Metals for Emergence of Energy Storage in Fuel Cells through Hydrogen Adsorption on the MgAl Surface. *Russ. J. Phys. Chem. B* 2024, 18 (2), 398–418.
- 32. F. Mollaamin. Competitive Intracellular Hydrogen-Nanocarrier Among Aluminum, Carbon, or Silicon Implantation: a Novel Technology of Eco-

- Friendly Energy Storage using Research Density Functional Theory. *Russ. J. Phys. Chem. B* **2024**, 18 (3), 805–820.
- H. Che, J. Liu, H. Wang, et al. Rubidium and cesium ions as electrolyte additive for improving performance of hard carbon anode in sodium-ion battery. *Electrochem. commun.* 2017, 83, 20–23.
- G. Henkelman, A. Arnaldsson, H. Jónsson. A fast and robust algorithm for Bader decomposition of charge density. *Comput. Mater. Sci.* 2006, 36 (3), 354–360.
- 35. M.J. Frisch, G.W. Trucks, H.B. Schlegel, G.E. Scuseria, M.A. Robb. Gaussian 16, Revision C.01, Gaussian; Inc, Wallingford CT.
- E. Kavitha, N. Sundaraganesan, S. Sebastian. Molecular structure, vibrational spectroscopic and HOMO, LUMO studies of 4-nitroaniline by density functional method; Semichem Inc, Shawnee Mission, KS, 2010; Vol. 48.
- Z. Xu, C. Qin, Y. Yu, G. Jiang, L. Zhao. First-principles study of adsorption, dissociation, and diffusion of hydrogen on α-U (110) surface. AIP Adv. 2024, 14 (5), 55114.
- 38. F. Mollaamin. Designing novel nanomaterials for li-ion batteries: a physico-chemical study through hydrogen-powered horizons. *New Mater. Compd. Appl.* **2024**, 8 (3), 303–323.
- T. Lu, F. Chen. Multiwfn: A multifunctional wavefunction analyzer. J. Comput. Chem. 2012, 33 (5), 580–592.
- T. Lu. A comprehensive electron wavefunction analysis toolbox for chemists, Multiwfn. J. Chem. Phys. 2024, 161 (8), 82503.
- 41. H.L. Schmider, A.D. Becke. Chemical content of the kinetic energy density. *J. Mol. Struct. THEOCHEM* **2000**, 527 (1–3), 51–61.
- G. Zhang, X. Gai, L. Sun, J. Ma. Determine the Relative Aromaticity of Bilayer Graphyne, Bilayer Graphdiyne, and Bilayer Graphtriyne. *Molecules* 2025, 30 (2).
- H. Guan, H. Sun, X. Zhao. Application of Density Functional Theory to Molecular Engineering of Pharmaceutical Formulations. *Int. J. Mol. Sci.* 2025, 26 (7), 3262.
- V. Tsirelson, A. Stash. Analyzing experimental electron density with the localized-orbital locator. *Acta Crystallogr. Sect. B Struct. Sci.* 2002, 58 (5), 780–785.